

Supporting Information

High Fluorescence Rate as a Key for Stable Blue Organic Light-Emitting Diodes

*Zhusen Liu,[§] Fangyi Cao,[§] Taiju Tsuboi, Yan Yue, Chao Deng, Xufeng Ni, Weilin Sun, Qisheng Zhang**

[*] Prof. Q. Zhang, Z. Liu, Dr. F. Cao, Prof. T. Tsuboi, Y. Yue, Dr. C. Deng, Prof. X. Ni, Prof. W. Sun

MOE Key Laboratory of Macromolecular Synthesis and Functionalization, Department of Polymer Science and Engineering, Zhejiang University, Hangzhou 310027, P.R. China

*E-mail: qishengzhang@zju.edu.cn

[§] These authors contributed equally.

Contents

1. Supplemental Tables and Figures
2. Materials and Synthesis
3. Relationship between SSA and Degradation
4. Relationship between LT50 and Decomposition Rate (C)
5. References

1. Supplemental Tables and Figures

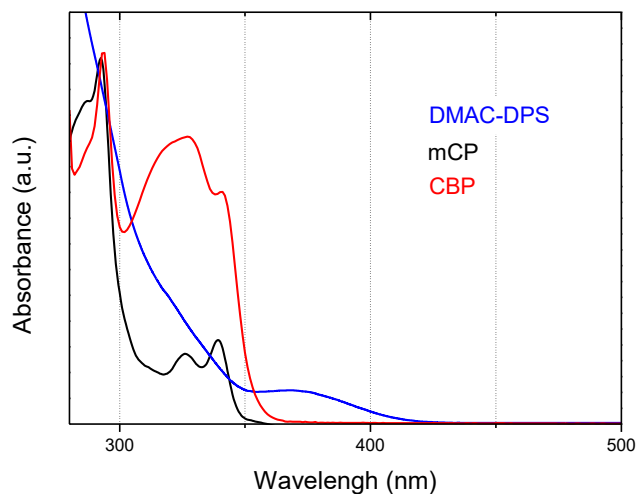


Figure S1. Ultraviolet–visible absorption spectra of DMAC-DPS, mCP and CBP in toluene solution at 300 K.

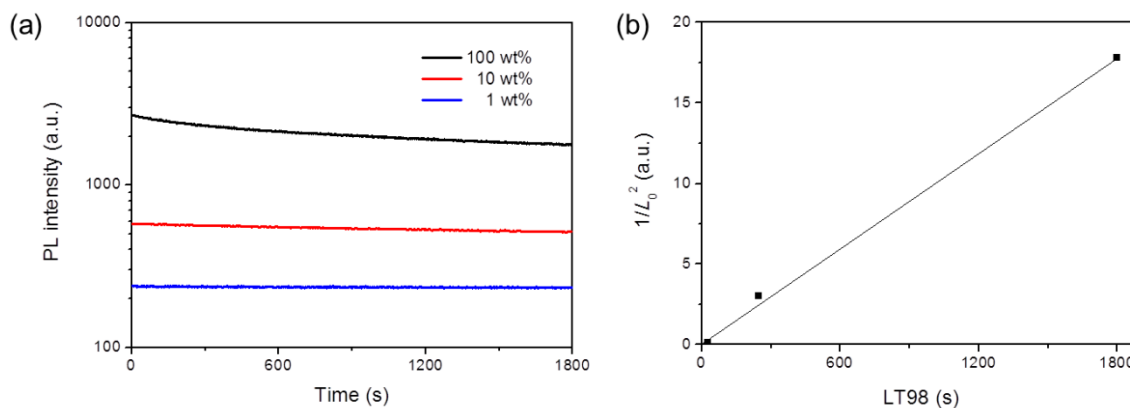


Figure S2. (a) Time dependence of the PL intensity for DMAC-DPS in doped mCP films (1 wt% and 10 wt%) and non-doped film (100 wt%) under 380 nm light; (b) The relationship between the initial luminance (L_0) of DMAC-DPS films and LT98 (time to 98% of initial luminance).

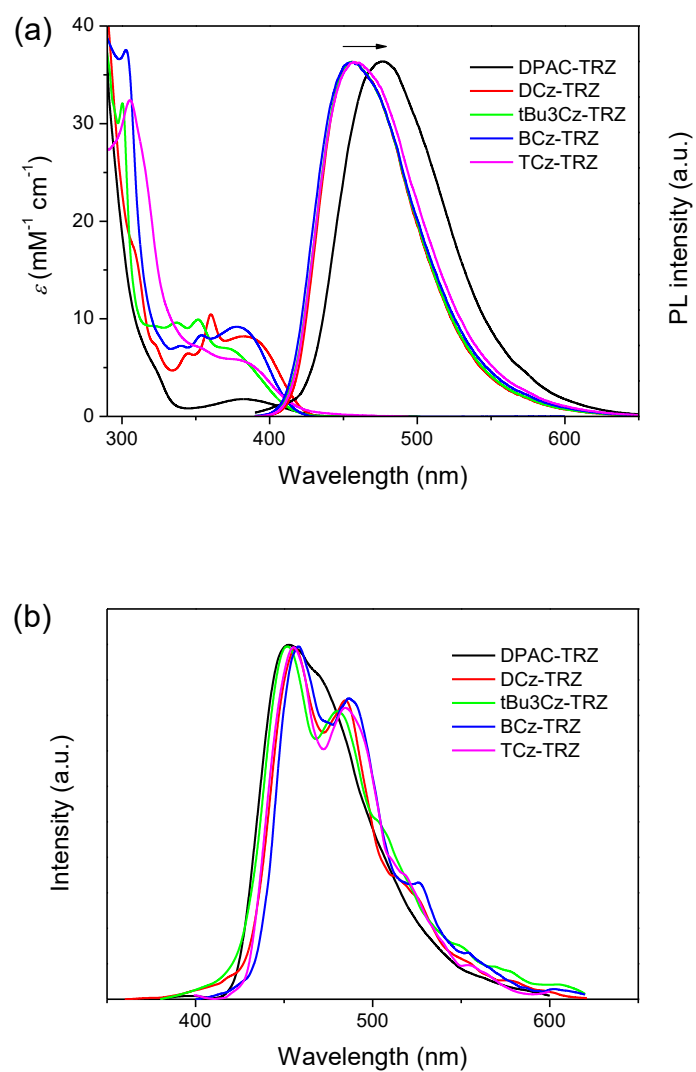


Figure S3. (a) Ultraviolet–visible absorption and emission spectra of the investigated molecules in toluene (2×10^{-5} M) at 300 K; (b) Phosphorescent spectra of the investigated molecules in toluene at 77 K.

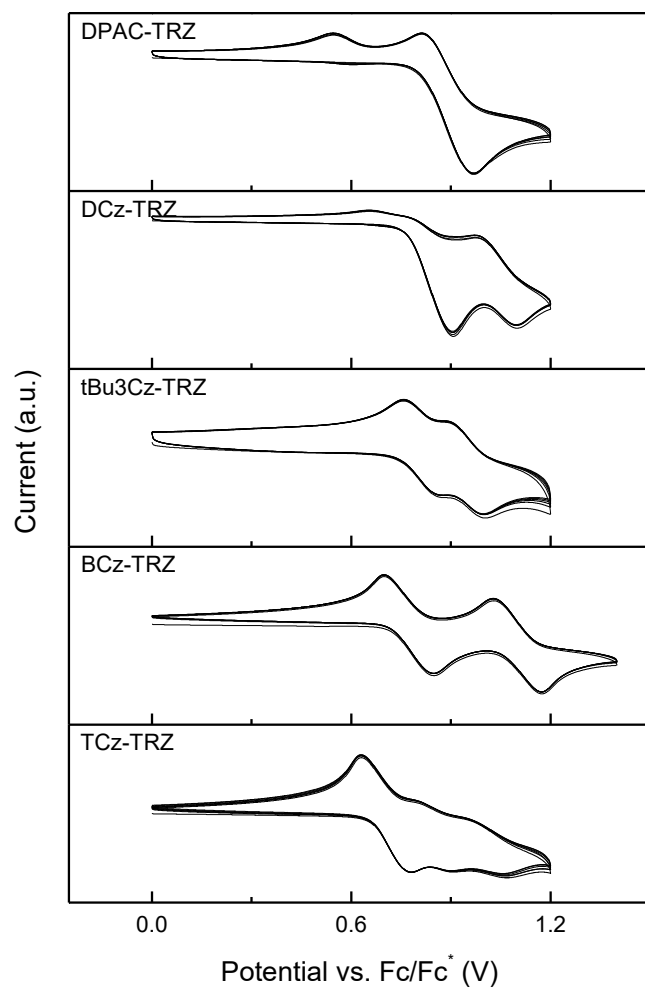


Figure S4. Multiple scan cyclic voltammograms for the oxidation of the investigated molecules in dichloromethane solutions at 300 K. Scan rate 100 mV s⁻¹ in 0.1 M TBAP.

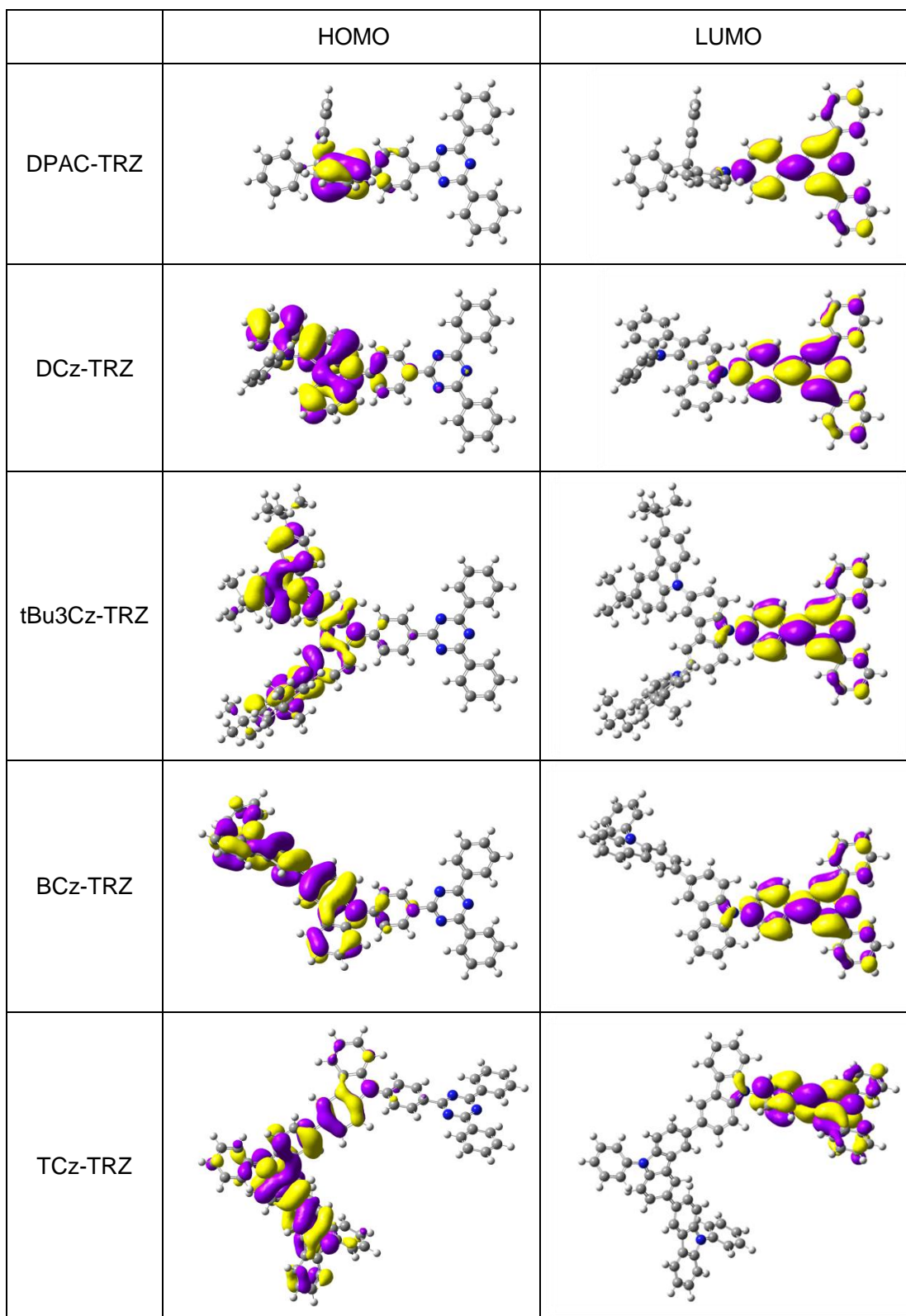


Figure S5. HOMO and LUMO of the investigated molecules in their S_0 state in vacuum.

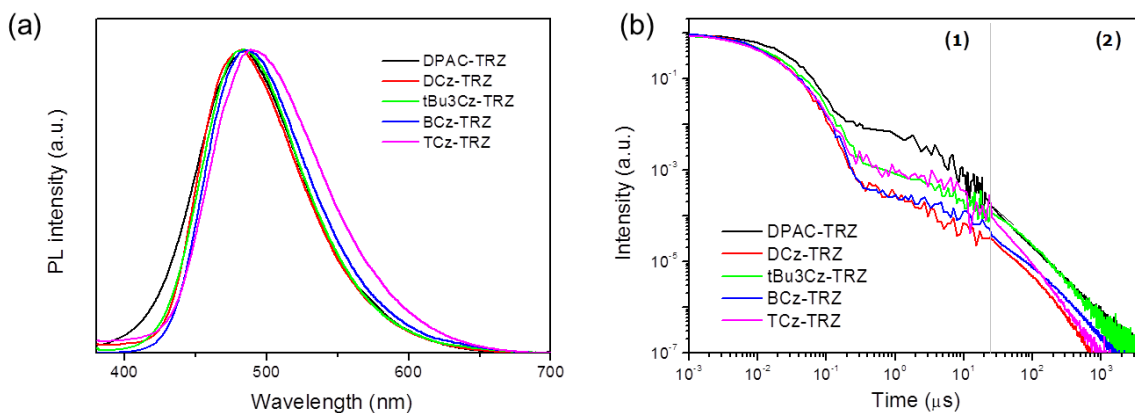


Figure S6. Steady-state (a) and transient (b) PL spectra of the investigated molecules doped into DPEPO films with a concentration of 20 wt% at 300 K. The transient measurement in the time ranges of (1) and (2) was performed by Lstroke mode and Lphos mode, respectively.

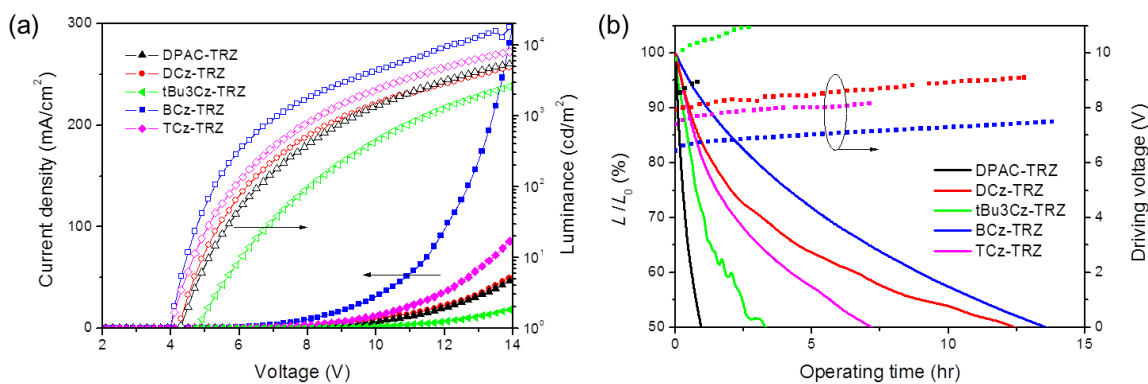


Figure S7. (a) Current density–voltage–luminance characteristics of the devices with a type I structure. (b) Luminance–voltage–operating time characteristics at fixed current densities for devices with a type I structure. The initial luminance is 500 cd/m².

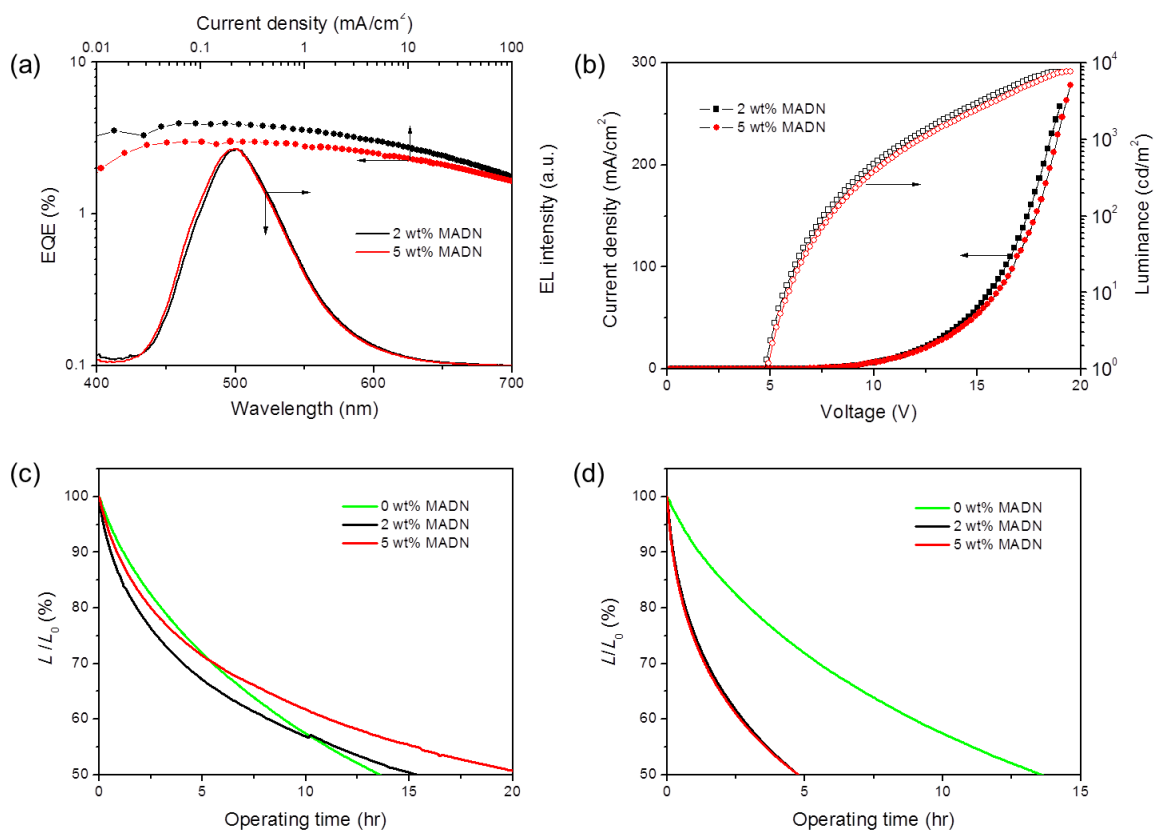


Figure S8. Performance of the OLEDs with a type I structure and MADN doped EML. (a) EQE versus current density (top and left axis) and EL spectra at 2 mA/cm². (b) Current density–voltage–luminance characteristics. (c) Half-life at a fixed current density of 0.16 mA cm⁻². (d) Half-life at a fixed current density with an initial luminance of 500 cd/m².

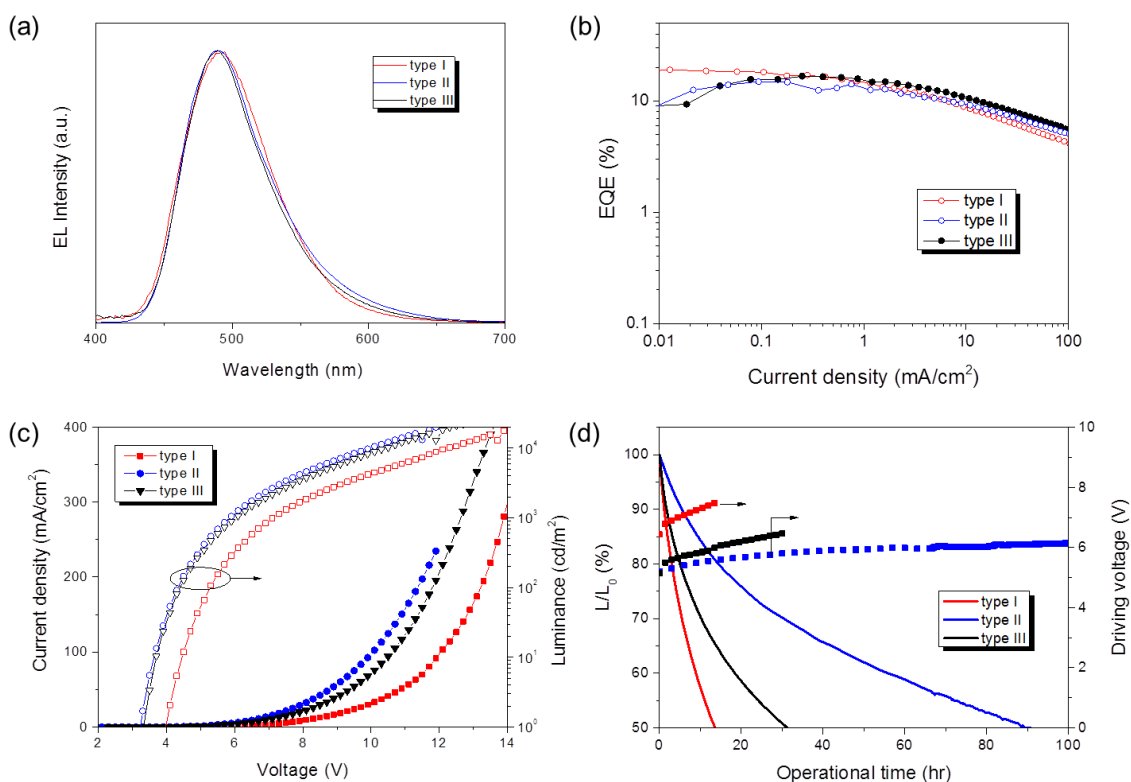


Figure S9. Performance of three types of OLEDs containing BCz-TRZ. The structure of type III: ITO/HAT-CN(7 nm)/ α -NPD(30 nm)/TCTA(15 nm)/ mCBP(15 nm)/BCz-TRZ: DPEPO(30 wt%, 30 nm)/DPEPO(3 nm)/TPBi(40 nm)/Liq(2 nm)/Al(100 nm) (a) EL spectra at 2 mA/cm². (b) EQE-current density characteristics of the devices. The EQE roll-off in type II and III OLEDs is less than that in type I one, because increasing the doping concentration of bipolar BCz-TRZ from 20 wt% to 30 wt% can improve the charge-carrier balance in the emitting layer employing n-type host DPEPO. (c) Current density-voltage-luminance characteristics of the devices. (b) Luminance-voltage-operational time characteristics of the devices at fixed current densities. The initial luminance is 500 cd/m².

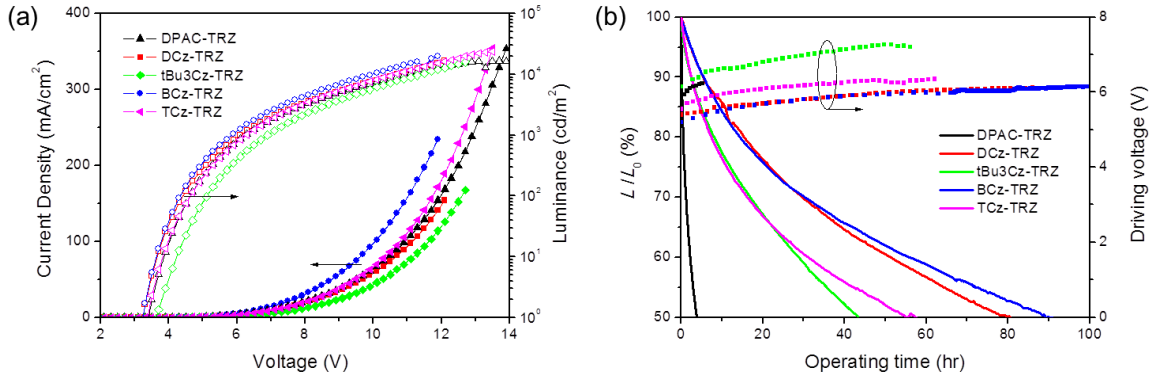


Figure S10. (a) Current density–voltage–luminance characteristics of the devices with a type II structure. (b) Luminance–voltage–operating time characteristics at fixed current densities for devices with a type II structure. The initial luminance is 500 cd/m².

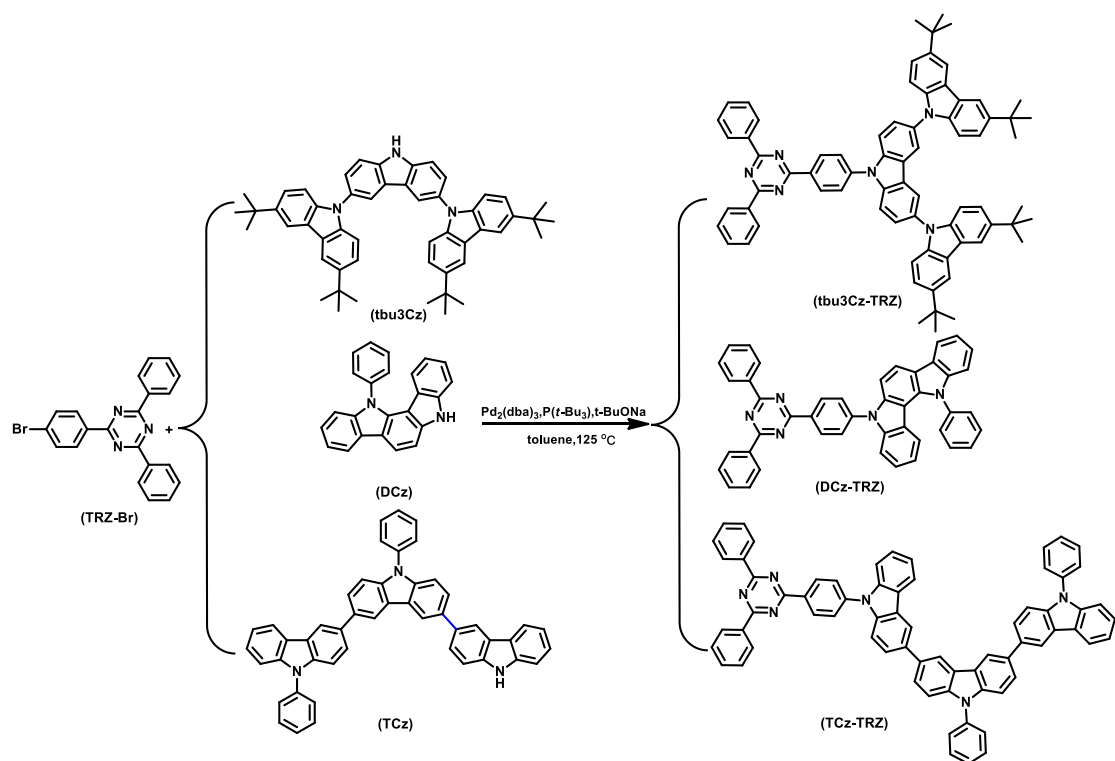
Table S1. Emission maxima (λ_{\max}), CIE coordinates, Turn-on voltages (V_{on}), maximum luminance (L_{\max}), maximum EQE (EQE_{\max}), EQE at 500 cd/m² (EQE_{500}), and LT50 for the devices with type I and II structures.

emitter	λ_{\max} (nm)	CIE	V_{on} (V)	L_{\max} (cd/m ²)	EQE_{\max} (%)	EQE_{500} (%)	LT50 (hr)
Type I							
DPAC-TRZ	488	0.16, 0.34	4.3	8800	15.8	11.6	1.0
DCz-TRZ	486	0.15, 0.31	4.3	11360	19.1	12.4	12.5
tBu3Cz-TRZ	486	0.16, 0.33	4.9	12100	16.2	11.6	3.2
BCz-TRZ	487	0.17, 0.34	4.0	17800	19.2	13.3	13.6
TCz-TRZ	491	0.16, 0.33	4.1	13700	17.5	13.8	7.2
Type II							
DPAC-TRZ	486	0.15, 0.34	3.5	16590	12.0	10.6	4
DCz-TRZ	492	0.16, 0.38	3.3	21640	15.5	12.6	80
tBu3Cz-TRZ	491	0.17, 0.38	3.7	24400	12.8	11.7	43
BCz-TRZ	490	0.18, 0.37	3.3	26450	14.4	12.9	90
TCz-TRZ	493	0.17, 0.37	3.5	23840	14.0	12.2	55

2. Materials and synthesis

General: All solvents and starting materials were purchased from commercial resources and were used as received unless otherwise stated. 10-(4-(4,6-diphenyl-1,3,5-triazin-2-yl)phenyl)-9,9-diphenyl-9,10-dihydroacridine (DPAC-TRZ),^[1] 9-(4-(4,6-diphenyl-1,3,5-triazin-2-yl)phenyl)-9'-phenyl-9H,9'H-3,3'-bicarbazole (BCz-TRZ),^[1] 3,3'',6,6''-tetra-tert-butyl-9'H-9,3':6',9''-tercarbazole (tBu3Cz)^[2] and 2-(4-bromo-phenyl)-4,6-diphenyl-1,3,5-triazine (TRZ-Br)^[3] were obtained by procedures given in the literature. The intermediates 12-phenyl-5,12-dihydroindolo[3,2-a]carbazole (DCz) and 9,9'-diphenyl-9H,9'H,9''H-3,3':6',3''-tercarbazole (TCz) were purchased from Xi'an Oder Photoelectronic Materials Co., Ltd. and were used without further purification. The host material DPEPO was prepared following procedures in the literature and was further purified by sublimation twice.^[4] HAT-CN, NPB, TCTA, mCBP, TPBi, and Liq were purchased from Jilin Optical and Electronic Materials Co., Ltd. and were used without further purification.

Nuclear magnetic resonance spectroscopy (NMR) were recorded on a Bruker Avance III 400 spectrometer (¹H: 400 MHz and ¹³C: 100 MHz) at room temperature using CDCl₃ as solvent and tetramethylsilane (TMS) as internal reference. Mass spectra measurements were performed on IT-TOF (Shimadzu, Japan) equipped with an ESI source in positive ion mode. Accurate mass determination was corrected by calibration using the sodium trifluoroacetate clusters as reference. Elemental analyses (C, H, N) were carried out with a Vario MICRO cube (Elementar).



Scheme S1. Molecular structures and synthesis of tBu3Cz-TRZ, DCz-TRZ and TCz-TRZ.

3,3'',6,6''-tetra-tert-butyl-9'-(4-(4,6-diphenyl-1,3,5-triazin-2-yl)phenyl)-9'H-9,3':6',9''-tercarbazole (tBu3Cz-TRZ)

A mixture of 2-(4-bromophenyl)-4,6-diphenyl-1,3,5-triazine (TRZ-Br, 0.75 g, 1.93 mmol), 3,3'',6,6''-tetra-tert-butyl-9'H-9,3':6',9''-tercarbazole (tBu3Cz, 1.67 g, 2.32 mmol), tris(dibenzylideneacetone)dipalladium (88.4 mg, 0.097 mmol), tri-*t*-butylphosphonium (39.0 mg, 0.193 mmol) and sodium tert-butoxide (0.37 g, 3.87 mmol) in 30 ml of toluene in a 100-ml three-necked flask were refluxed for 12 hours under argon. The mixture was extracted with dichloromethane. The combined organic extracts were dried over Na₂SO₄ and concentrated by rotary evaporation. The crude product was purified by column chromatography on silica gel using 1:10 dichloromethane/petroleum as eluent to afford a yellow solid tBu3Cz-TRZ (1.67 g, 84%). ¹H NMR (400 MHz, CDCl₃, 25 °C, TMS δ in ppm) δ = 9.13 (d, *J* = 8.4 Hz, 2H), 8.85 (dd, ¹*J* = 7.6 Hz, ²*J* = 2.0 Hz, 4H), 8.27 (d, *J* = 1.6 Hz, 2H), 8.17 (d, *J* = 1.6 Hz, 4H), 7.99 (d, *J* = 8.4 Hz, 2H), 7.79 (d, *J* = 8.4 Hz, 2H), 7.67–7.60 (m, 8H), 7.49–7.46 (m, 4H), 7.38–7.35 (m, 4H), 1.47 (s, 36H); ¹³C NMR (100 MHz, CDCl₃, 25 °C, TMS δ in ppm) δ = 171.9, 142.6, 141.1, 140.1, 140.0,

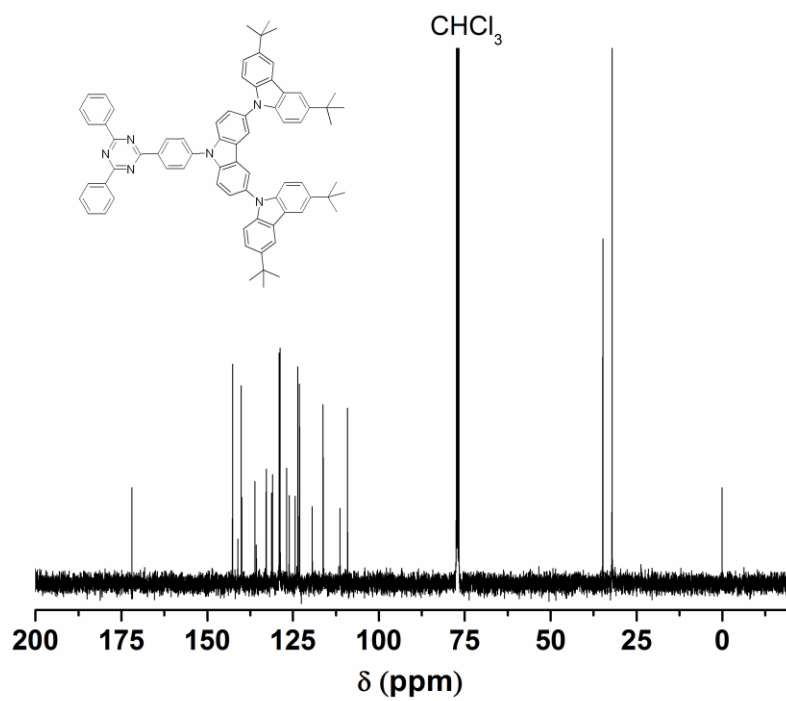
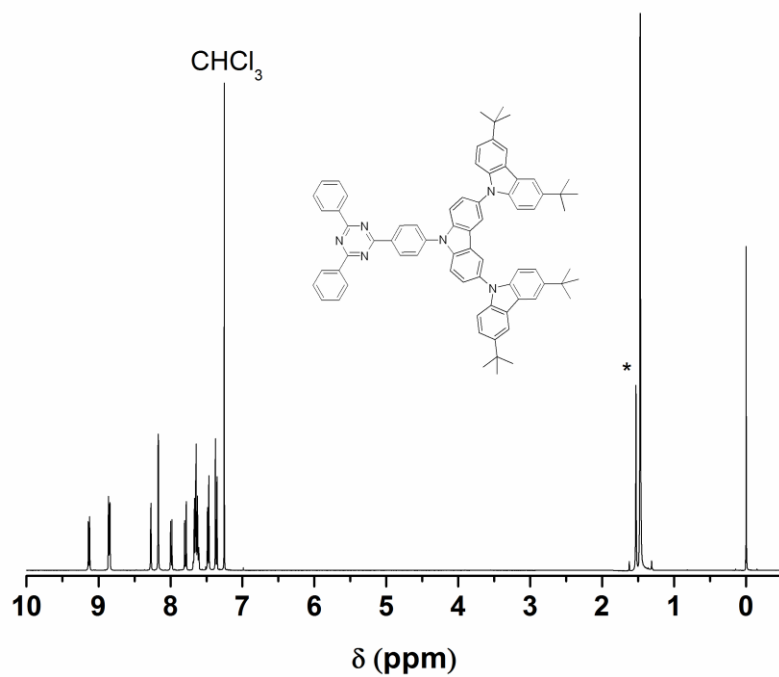
136.1, 135.7, 132.8, 131.3, 131.0, 129.1, 128.8, 126.9, 126.2, 124.4, 123.6, 123.2, 119.4, 116.3, 111.3, 109.1, 34.8, 32.1, ppm; Anal. calcd for C₇₃H₆₈N₆ (%):C, 85.18; H, 6.66; N, 8.16; found: C, 85.18; H, 6.67; N, 8.18.

5-(4-(4,6-diphenyl-1,3,5-triazin-2-yl)phenyl)-12-phenyl-5,12-dihydro-indolo[3,2-a]carbazole (DCz-TRZ)

A procedure similar to that used for tBu3Cz-TRZ was followed but with DCz (0.77 g, 2.32 mmol) instead of tBu3Cz after evaporation of toluene, the crude product was subjected to column chromatography on silica gel using 1:10 dichloromethane /petroleum as eluent to afford a light yellow solid with a yield of 76%. **¹H NMR** (400 MHz, CDCl₃, 25 °C, TMS δ in ppm) δ = 9.05 (d, *J* = 8.8 Hz, 2H), 8.83 (dd, ¹*J* = 8.0 Hz, ²*J* = 1.2 Hz, 4H), 8.22–8.15 (m, 2H), 7.84 (d, *J* = 8.4 Hz, 2H), 7.67–7.59 (m, 11H), 7.45 (t, *J* = 8.4 Hz, 2H), 7.38–7.27 (m, 4H), 6.83 (t, *J* = 7.2 Hz, 1H), 5.97 (d, *J* = 8.4 Hz, 1H); **¹³C NMR** (100 MHz, CDCl₃, 25 °C, TMS δ in ppm) δ = 171.9, 171.0, 142.0, 141.7, 141.2, 140.4, 140.0, 136.9, 136.1, 135.6, 132.7, 130.7, 130.0, 129.3, 129.1, 128.8, 128.5, 127.9, 124.6, 124.4, 124.3, 123.7, 121.8, 120.5, 119.8, 199.0, 118.7, 117.8, 110.2, 109.3, 108.2, 103.6 ppm; HRMS (ESI): calculated for 662.2 (C₄₅H₂₉N₅ + Na⁺), found: 662.2. Anal. calcd for C₄₅H₂₉N₅ (%):C, 84.48; H, 4.57; N, 10.95; found: 84.46; H, 4.66; N, 10.93.

9-(4-(4,6-diphenyl-1,3,5-triazin-2-yl)phenyl)-9',9''-diphenyl-9H,9'H,9''H-3,3':6',3''-tercarbazole (TCz-TRZ)

A procedure similar to that used for tBu3Cz-TRZ was followed but with TCz (1.51 g, 2.32 mmol) instead of tBu3Cz after evaporation of the solvent, the crude product was subjected to column chromatography on silica gel using 1:15 ethyl acetate/petroleum as eluent to afford a khaki solid with a yield of 68%. **¹H NMR** (400 MHz, CDCl₃, 25 °C, TMS δ in ppm) δ = 9.03–8.81 (m, 5H), 8.58–8.49 (m, 4H), 8.26 (t, *J* = 7.6 Hz, 2H), 7.86–7.78 (m, 6H), 7.66–7.31 (m, 27H); **¹³C NMR** (100 MHz, CDCl₃, 25 °C, TMS δ in ppm) δ = 171.8, 170.9, 141.7, 141.4, 140.9, 140.5, 140.5, 140.1, 139.6, 137.9, 137.8, 136.2, 134.9, 134.8, 134.5, 134.3, 134.2, 132.7, 130.7, 130.0, 130.0, 129.1, 128.8, 127.5, 127.1, 127.0, 126.6, 126.3, 126.1, 126.0, 126.0, 125.9, 124.5, 124.3, 124.2, 124.1, 124.0, 123.6, 120.7, 120.6, 120.5, 120.0, 119.0, 118.9, 110.2, 110.1, 109.9 ppm; Anal. calcd for C₆₉H₄₄N₆ (%):C, 86.59; H, 4.63; N, 8.78; found: C, 86.71; H, 4.72; N, 8.63.



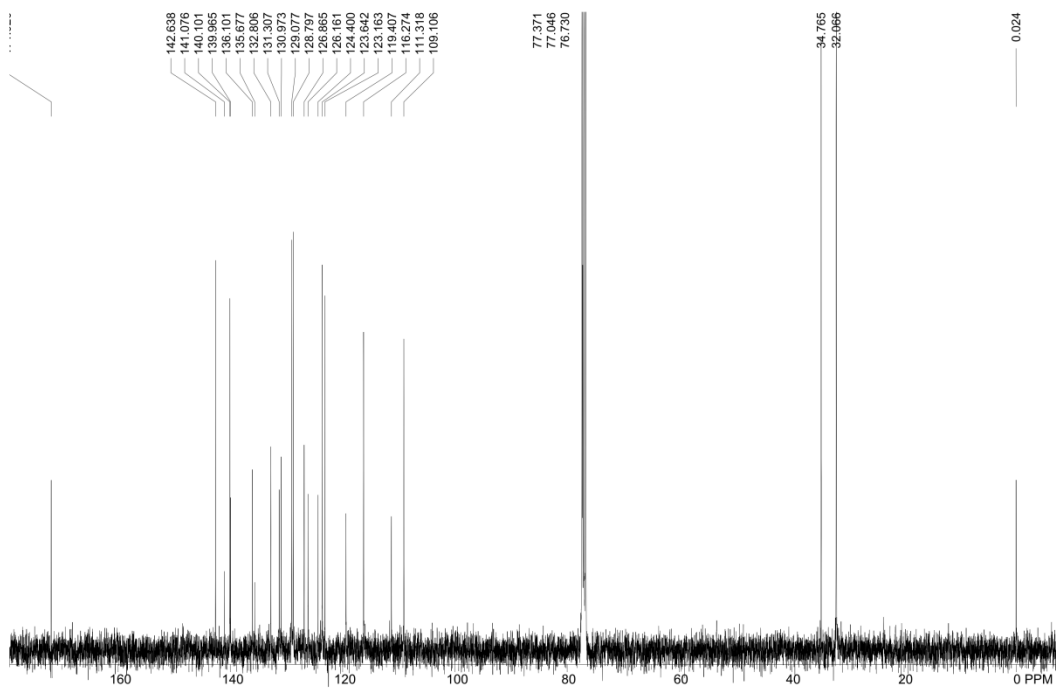
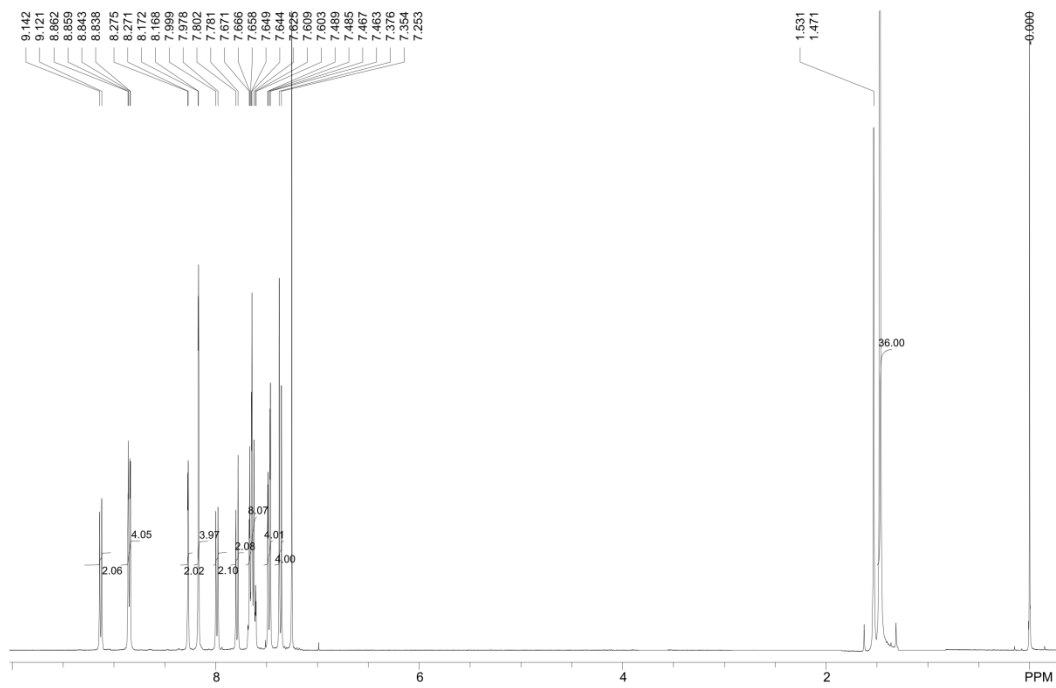
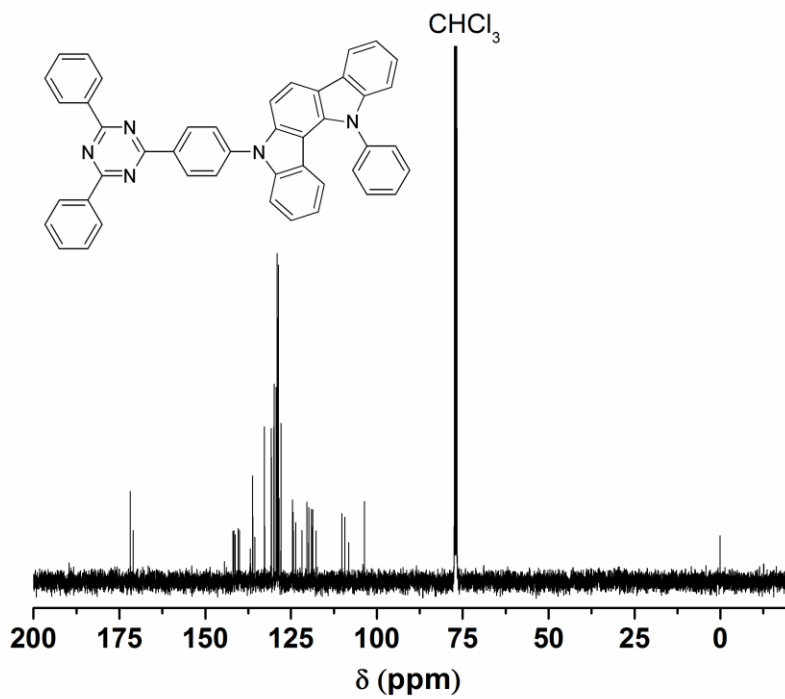
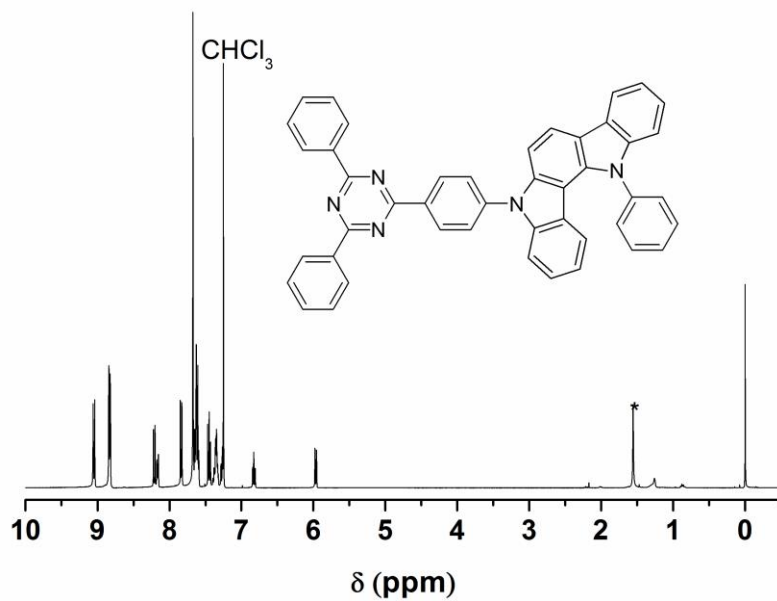


Figure S11. ^1H NMR and ^{13}C NMR spectra of tbu3Cz-TRZ, *: water.



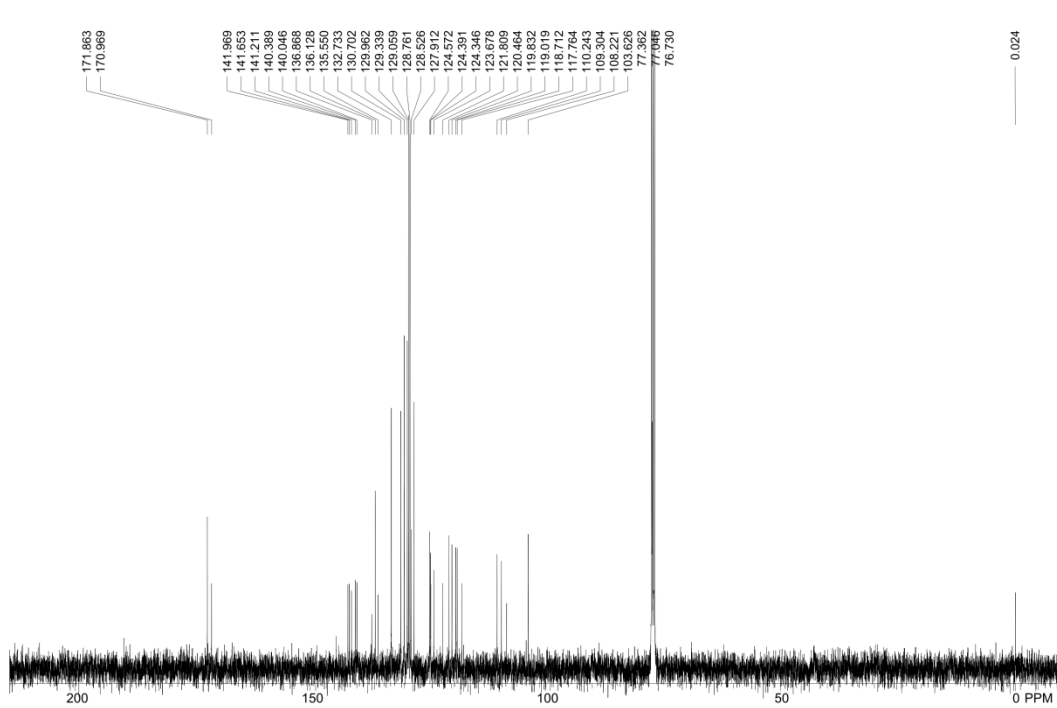
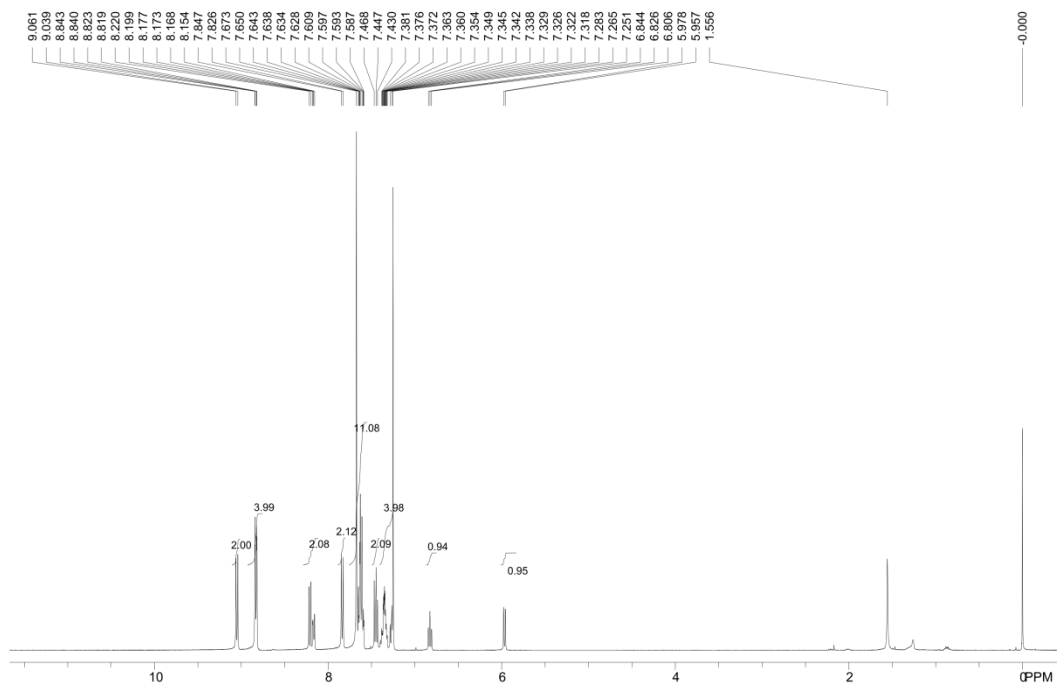
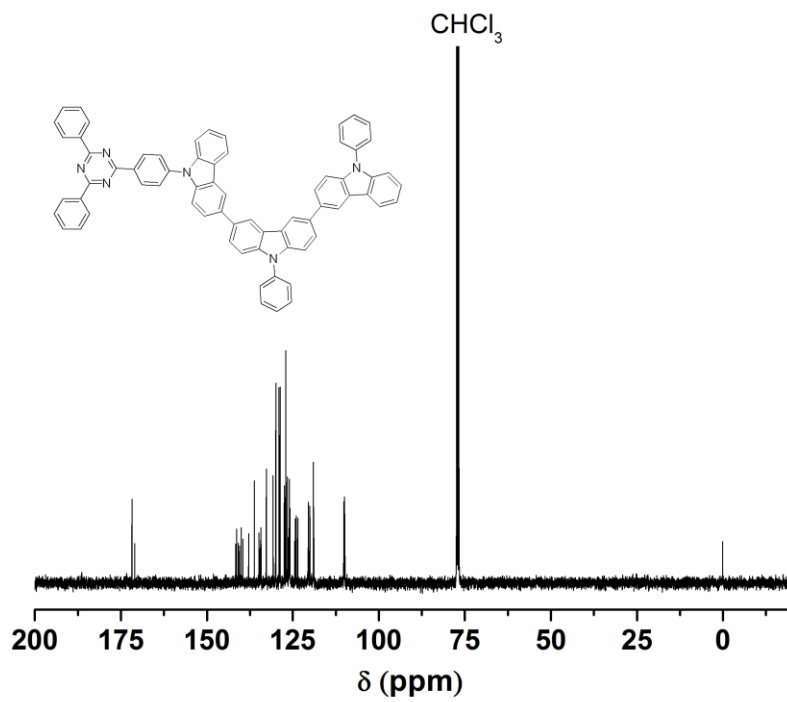
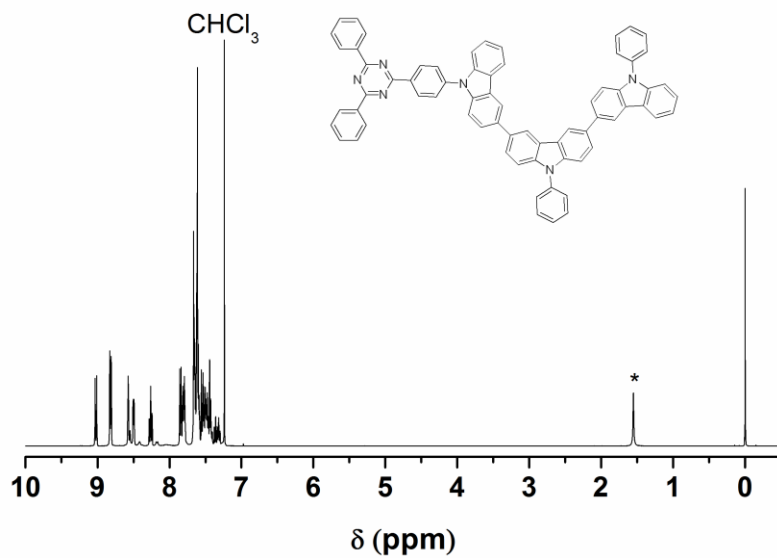


Figure S12. ^1H NMR and ^{13}C NMR spectra of DCz-TRZ, *: water.



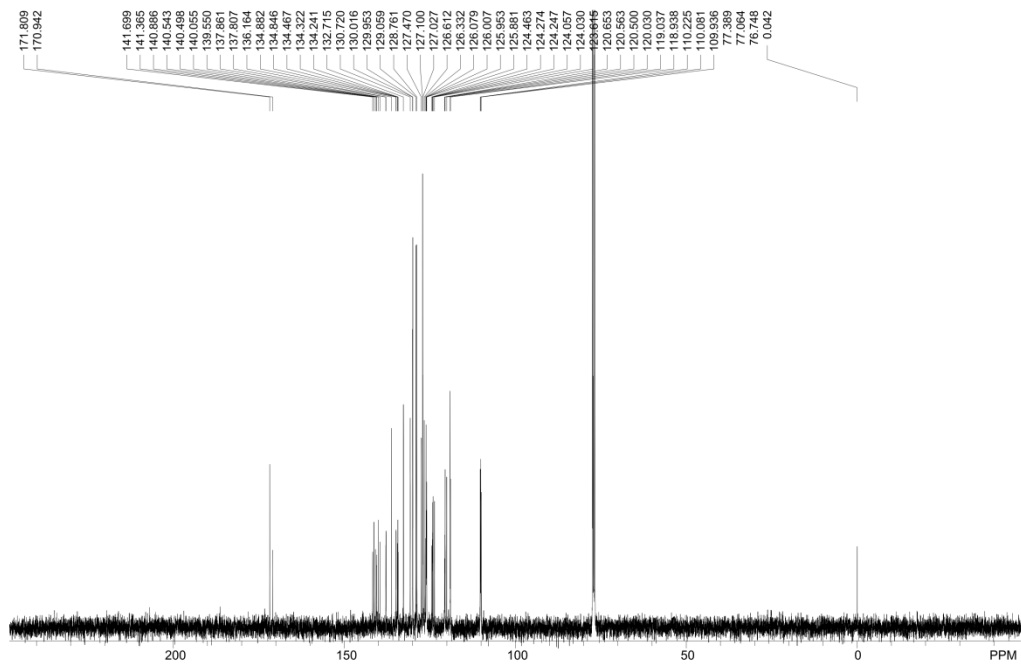
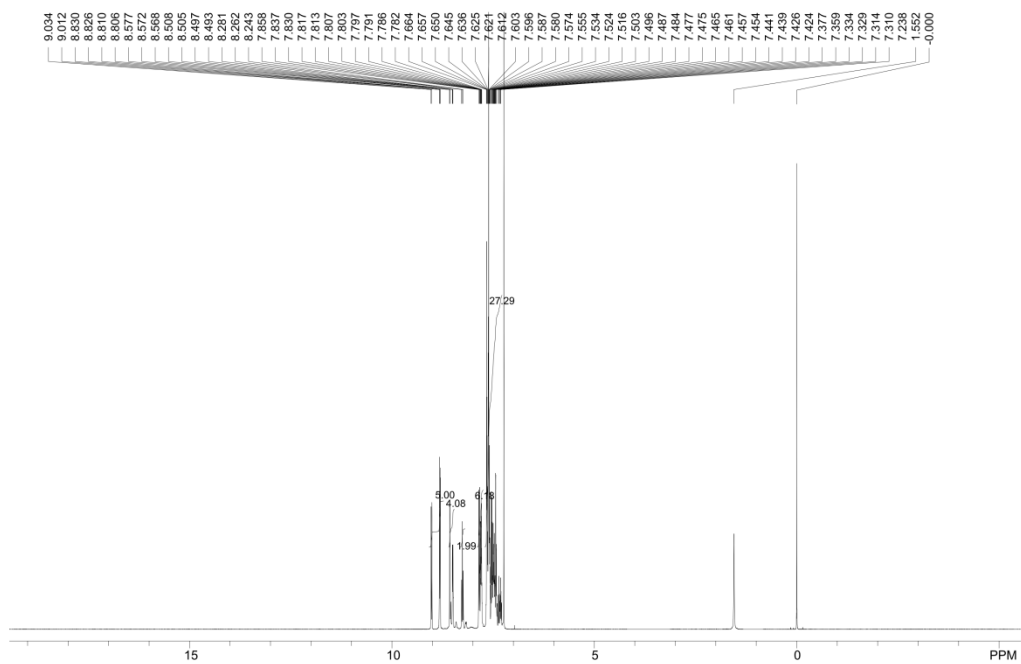
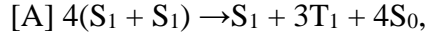


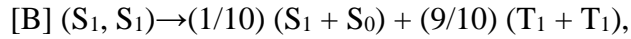
Figure S13. ^1H NMR and ^{13}C NMR spectra of TCz-TRZ, *: water.

3. Relationship between SSA and Degradation

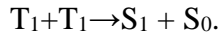
Singlet–singlet annihilation (or called singlet fusion) appears in a pair of two emitting monomers excited into the S_1 state. Currently the following two processes are suggested.



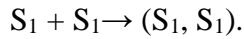
where S_1 and T_1 mean the excited singlet and triplet states, respectively,^[5,6] and



where (S_1, S_1) represents excimer.^[7] Another process is also conceivable for SSA from the analogy to the cooperative excitation TTA (triplet-triplet annihilation), which is given by



This additional process consists of two processes. The first process is a formation of excimer-like virtual state (S_1, S_1) in the pair by the electric excitation (this corresponds to the case of our degradation measurement for 20 % and 30 % TADF emitters in EML)



The excimer energy is located at the twice the energy of the S_1 state. The second process is the energy transfer from the excimer state to (1) nearby the S_n state of the neighboring monomer, which leads to the S_1 emission after the non-radiative relaxation $S_n \rightarrow S_1$, or (2) nearby unintentionally doped impurities such as oxygen, water and defect, which lead to EL degradation of OLEDs (**Figure S14**).

These two processes compete with each other in the EML. If the rate of the latter process is higher than the former one, short LT50 is observed, while long LT50 is observed in case of much lower rate for the latter rate. In the present paper we propose the process of **Figure S14**.

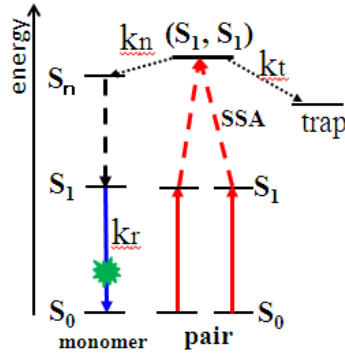


Figure S14. Schematic energy level diagram and the SSA process followed by several relaxation processes. The rates k_t , k_n and k_r are the relaxation rates to the trap centers, the S_n state of the monomer (non-radiative), and the ground state (generating emission), respectively. The TADF emitters have several broad absorption bands in the UV range, suggesting the presence of the S_n state energetically close to the (S_1, S_1) excimer state. This process does not lead the EL degradation. The observed degradation is understood by the destruction of TADF emitters by the k_t process to the trap centers through the SSA. Oxygen molecule, which has been considered as the main trap in the EML of OLED, has the energy levels in the UV-Vis range (e.g., at 3.26 eV ($^1\Sigma_g^+$) and 2.60 eV ($^1\Delta_g + ^1\Sigma_g^+$)). Therefore energy transfer to the O_2 molecule is not negligible.

4. Relationship between LT50 and Decomposition Rate (C)

The degradation measurement shows nearly a single exponential decay until time of LT50. Exactly speaking it would follow a stretched exponential decrease of the luminance with degradation time $L(t)=L_0 \exp(-(t/\tau)^\beta)$ for a wide time range, where L_0 means luminance at $t=0$, *i.e.*, the initial luminance of OLED.^[8-10] SSA process gives a reduction of TADF emitters, which leads to degradation of EL from OLED. SSA is caused by TADF molecule-pair. The observed exponential degradation is obtained from the following rate equation for the number of this pairs [SS].

$$d[SS]/dt = -C[SS]$$

Here C is the decomposition rate. This equation gives a decay time $\tau_{1/e} = 1/C$.

$$LT50 = (\ln 2)\tau_{1/e} = (\ln 2)/C \quad (9)$$

The parameters L in Eq. (8) are time-dependent. Eq. (8) at a time of LT50 is expressed by

$$C = 8\pi cRD_S \left(\frac{L_0}{2aew\eta_{out}k_F} \right)^2 \quad (10)$$

Eq. (10) indicates that C is inversely proportional to k_F^2 . Therefore Eq. (9) leads to $LT50 \propto k_F^2$.

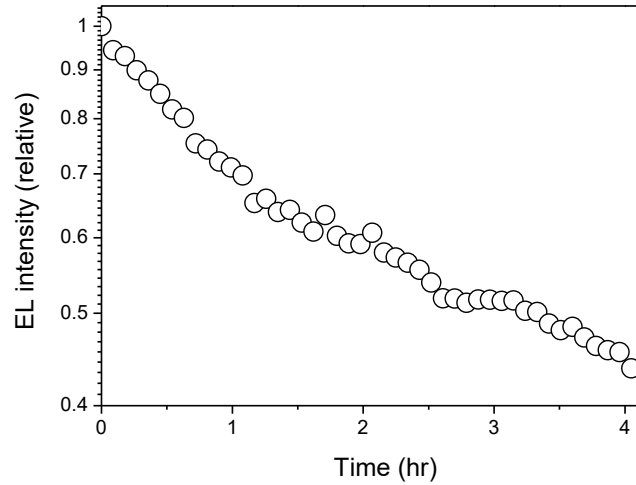


Figure S15 EL degradation of tBuCz-TRZ based OLED with type I structure. The degradation follows nearly exponential law.

References

- [1] L.-S. Cui, Y.-L. Deng, D. P.-K. Tsang, Z.-Q. Jiang, Q. Zhang, L.-S. Liao, C. Adachi, *Adv. Mater.* **2016**, *28*, 7620.
- [2] a) T. Xu, R. Lu, X. Liu, X. Zheng, X. Qiu, Y. Zhao, *Org. Lett.* **2007**, *9*, 797; b) J. Ding, J. Lü, Y. Cheng, Z. Xie, L. Wang, X. Jing, F. Wang, *Adv. Funct. Mater.* **2008**, *18*, 2754; c) P. Moonsin, N. Prachumrak, R. Rattanawan, T. Keawin, S. Jungsuttiwong, T. Sudyoadsuk, V. Promarak, *Chem Comm* **2012**, *48*, 3382.
- [3] H. Tanaka, K. Shizu, H. Miyazaki, C. Adachi, *Chem. Comm.* **2012**, *48*, 11392.

- [4] J. Fawcett, A. W. G. Platt, S. Vickers, M. D. Ward, *Polyhedron* **2004**, *23*, 2561.
- [5] M. A. Baldo, R. J. Holmes, S. R. Forrest, *Phys. Rev. B* **2002**, *66*, 035321.
- [6] H. Nakanotani, H. Sasabe, C. Adachi, *Appl. Phys. Lett.* **2005**, *86*, 213506.
- [7] A.P. Monkman, Hindawi Publishing Corporation, ISRN Mater. Sci. Vol. 2013, Article ID 670130 (2013) <http://dx.doi.org/10.1155/2013/670130>
- [8] F. So and D. Kondakov, *Adv. Mater.* **2010**, *22*, 3762.
- [9] C. Féry, B. Racine, D. Vaufrey, H. Doyeux, S. Cinà, *Appl. Phys. Lett.* **2005**, *87*, 213502.
- [10] T. D. Schmidt, Dissertation “Photophysics of organic light-emitting diodes :Device efficiency and degradation processes” (2013, Universität Augsburg)